Two-stream instability for a longitudinally compressing charged particle beam

Edward A. Startsev and Ronald C. Davidson
Plasma Physics Laboratory, Princeton University, Princeton, New Jersey 08543

(Received 28 March 2006; accepted 19 May 2006; published online 21 June 2006)

The electrostatic two-stream instability for a cold, longitudinally compressing charged particle beam propagating through a background plasma has been investigated both analytically and numerically. Small-signal coupled equations describing the evolution of the perturbations are derived, and the asymptotic solutions are obtained. The results are confirmed by direct numerical solution of the linearized fluid equations. It is found that the longitudinal beam compression strongly modifies the space-time development of the instability. In particular, the dynamic compression leads to a significant reduction in the growth rate of the two-stream instability compared to the case without an initial velocity tilt. © *2006 American Institute of Physics*. [DOI: 10.1063/1.2212807]

I. INTRODUCTION

To achieve the high focal spot intensities necessary for high energy density physics and heavy ion fusion applications, the ion beam pulse must be compressed longitudinally by factors of 10–100 before it is focused onto the target. The longitudinal compression is achieved by imposing an initial velocity profile tilt on the drifting beam in vacuum.[1–3] To achieve maximum longitudinal compression, the space charge of the beam is neutralized by propagation through a dense neutralizing background plasma.[2–5] If the space charge is fully neutralized by the plasma, the final compression is limited only by the initial longitudinal temperature of the beam ions and possible collective processes (such as the two-stream instability[6–9]) which may prevent full neutralization. The beam's longitudinal thermal spread which could stabilize the instability also inhibits full longitudinal compression. Therefore, in this paper, we make use of a macroscopic fluid model[10] to investigate both analytically and numerically the electrostatic two-stream instability for a cold, longitudinally compressing charged particle beam propagating through a background plasma. It is found that the longitudinal beam compression alone strongly modifies the space-time development of the two-stream instability. In particular, it is found that the dynamic compression leads to a significant reduction in the growth rate of the two-stream instability compared to the case without an initial velocity tilt.

The analysis presented here is similar to the analysis for a uniform infinite beam pulse.[6] In that case it is well known that the propagation of a cold beam through a cold, background plasma is absolutely unstable. The effects that limit the instability growth are the thermal spread of the beam particles and possible density gradients.[11] In the case considered here, the instability growth is limited by the velocity tilt. Indeed, for small beam density, the instability requires that the resonance condition $\omega = kV_b \approx \omega_{pe}$ be satisfied for a continuous growth. Here ω_{pe} is the electron plasma frequency associated with the plasma electrons, k is the axial wave number of the perturbation, and V_b is the beam velocity. As shown in Sec. V, the perturbation frequency changes with time due to the time-dependent beam velocity and beam density profile, and it eventually detunes out of resonance and the instability ceases. The present analysis takes into account the effects of the velocity tilt and allows the level of saturation to be determined. A similar analysis has been used to study the filamentation instability for a radially converging heavy ion beam.[12] The effects of radial convergence on the two-stream instability has also been studied.[13,14] Numerical simulations using the particle-in-cell code LSP have recently appeared in the literature that address the practical requirements for neutralized propagation of heavy-ion beams for cases with and without longitudinal compression.[3,5] Some preliminary numerical simulations of the possible effects of longitudinal compression on the two-stream instability for longitudinally compressing heavy-ion beams have also been reported.[3]

This paper is organized as follows: In Sec. II, we consider the unperturbed propagation of the electron beam in the background plasma. In Sec. III, small-signal equations are derived that describe the evolution of the density perturbations around the flow described by the unperturbed equations. In Sec. IV, we obtain the asymptotic solution of the resulting equations. In Sec. V, the development of the instability and its saturation are examined from the point of view of the wave dynamics, where the plasma waves are represented as quasiparticles characterized by their position $x(t)$, wave number $k(t)$ and energy (or frequency) $\omega(t)$. In Sec. VI, numerical solutions of the linearized equations are obtained and compared with the analytical results. Finally, the results are summarized in Sec. VII.

II. UNPERTURBED PROPAGATION

It is assumed that a semi-infinite electron beam with a sharp leading edge enters the chamber containing background plasma at time $t=0$ and $x=0$ with velocity V_b^0 and density n_b^0. The beam is uniformly compressing in the longitudinal direction as it propagates inside the chamber and reaches the maximum compression at time $t=T_f$ at the point $x=X_f=T_f V_b^0$ away from the beam entry point $x=0$ into the chamber. The unperturbed beam propagation is illustrated in

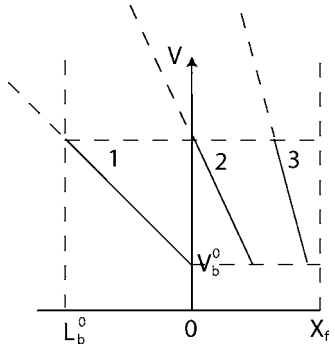

FIG. 1. Plot of the beam phase space at different times during the compression. Line 1 corresponds to $t=0$.

Fig. 1, where the beam phase space is plotted at different times during the compression. The transition from solid to dashed lines in Fig. 1 identifies the end of the real beam pulse with finite initial length L_b^0. The frequently used parameter, the longitudinal "velocity tilt" $\Delta V_b^0/V_b^0$, is related to the compression distance X_f and the initial beam pulse length L_b^0 by

$$\Delta V_b^0/V_b^0 = L_b^0/X_f. \tag{1}$$

It is also assumed that the electron beam propagation in the background plasma is both charge neutralized and current neutralized, where the quasineutrality conditions are given by

$$\bar{n}_e + \bar{n}_b = n_0, \tag{2}$$

$$\bar{n}_e \bar{V}_e + \bar{n}_b \bar{V}_b = 0. \tag{3}$$

Here, $\bar{n}_j$ and $\bar{V}_j$ denote the dynamically changing unperturbed density and flow velocity of the beam electrons ($j=b$) and background plasma electrons ($j=e$), and $n_0=$const. (independent of x and t) is the uniform density of the background plasma ions (assumed singly ionized). The quasineutrality condition is slightly violated due to the finite electron mass in the force balance equation for the plasma electrons

$$e\bar{E} = -m_e\left(\frac{\partial \bar{V}_e}{\partial t} + \bar{V}_e\frac{\partial \bar{V}_e}{\partial x}\right). \tag{4}$$

The zero-order solution for the beam density and velocity are given by

$$\bar{n}_b(t) = \frac{n_b^0 T_f}{T_f - t}, \tag{5}$$

$$\bar{V}_b(t,x) = \frac{V_b^0 T_f - x}{T_f - t}. \tag{6}$$

Here, it is also assumed that $\delta \equiv n_b^0/n_0 \ll 1$. Substituting Eqs. (2), (3), (5), and (6) into Eq. (4), we obtain for the unneutralized electric field

$$e\bar{E} = 2m_e\frac{n_b^0}{n_0}\frac{(X_f - x)}{[(1 - t/T_f) + (n_b^0/n_0)]^2 T_f(T_f - t)}. \tag{7}$$

Using Poisson's equation $\partial\bar{E}/\partial x = 4\pi e\,\delta\bar{n} = 4\pi e(\delta\bar{n}_b - \delta\bar{n}_e)$, we obtain for the unneutralized charge density

$$\frac{\delta\bar{n}(x,t)}{\bar{n}_b(t)} = -\frac{2}{\omega_{pe}^2 T_f^2}\frac{1}{\left[\left(1 - \frac{t}{T_f}\right) + \frac{n_b^0}{n_0}\right]^2}, \tag{8}$$

where $\omega_{pe}^2 \equiv 4\pi n_0 e^2/m_e$ is the plasma frequency-squared of the background plasma electrons. In what follows we make use of two small parameters

$$\epsilon \equiv 1/(\omega_{pe}T_f) \ll 1 \quad \text{and} \quad \delta \equiv n_b^0/n_0 \ll 1. \tag{9}$$

It will be shown that the resonant two-stream instability develops and saturates everywhere in the chamber except close to the compression point $x=X_f$ during the time interval when $1 - t/T_f \sim 1 \gg n_b^0/n_0$. It follows from Eq. (8) that $\delta\bar{n}(x,t)/\bar{n}_b(t) \simeq 2\epsilon^2$ during this time interval and therefore for perturbations with amplitude $|\delta\tilde{n}(x,t)|/\bar{n}_b(t) \gg \epsilon^2$, the beam can be considered as fully neutralized by the background plasma.

III. SMALL-SIGNAL EQUATIONS

In this section, we derive the coupled equations that describe the perturbation in charge density of the beam electrons and background electrons. Quantities are expressed as $n_b = \bar{n}_b + \tilde{n}_b$, $v_b = \bar{V}_b + \tilde{v}_b$, $n_e = \bar{n}_e + \tilde{n}_e$, $v_e = \bar{v}_e + \tilde{V}_e$ where unperturbed quantities $\bar{n}_b$, $\bar{V}_b$, $\bar{n}_e$, and $\bar{V}_e$ are determined from Eqs. (2), (3), (5), and (6). Substituting Eqs. (5) and (6) into the linearized continuity equation for the beam particles, we obtain

$$(T_f - t)\frac{\partial\tilde{n}_b}{\partial t} - \tilde{n}_b + (T_f V_b^0 - x)\frac{\partial\tilde{n}_b}{\partial x} = -T_f n_b^0\frac{\partial\tilde{v}_b}{\partial x}. \tag{10}$$

From the linearized momentum equation for the beam particles, we obtain

$$(T_f - t)\frac{\partial\tilde{v}_b}{\partial t} - \tilde{v}_b + (T_f V_b^0 - x)\frac{\partial\tilde{v}_b}{\partial x} = -\frac{e}{m_e}(T_f - t)\tilde{E}. \tag{11}$$

Here, E is linearized near $\bar{E}=0$. Combining Eqs (10) and (11), and introducing the normalized variables,

$$t\omega_{pe} = \bar{t}, \quad x\omega_{pe}/V_b^0 = \bar{x}, \quad \tilde{n}_b/n_0 = \tilde{\bar{n}}_b,$$
$$\tilde{v}_b/V_b^0 = \tilde{\bar{v}}_b \text{ and } e\tilde{E}/m_e\omega_{pe}V_b^0 = \tilde{\bar{E}}, \tag{12}$$

we obtain

$$[(1 - \epsilon\bar{t})\partial_{\bar{t}} + (1 - \epsilon\bar{x})\partial_{\bar{x}} - 2\epsilon]$$
$$\times[(1 - \epsilon\bar{t})\partial_{\bar{t}} + (1 - \epsilon\bar{x})\partial_{\bar{x}} - \epsilon]\tilde{\bar{n}}_b = \alpha^2\epsilon^2(1 - \epsilon\bar{t})\partial_{\bar{x}}\tilde{\bar{E}}$$
$$= -\alpha^2\epsilon^2(1 - \epsilon\bar{t})(\tilde{\bar{n}}_b + \tilde{\bar{n}}_e), \tag{13}$$

where $\alpha \equiv \omega_{pb}T_f$, and use has been made of Poisson's equation $\partial_{\bar{x}}\tilde{\bar{E}} = -\tilde{\bar{n}}_b - \tilde{\bar{n}}_e$.

Repeating the same procedure for the background plasma electrons, we obtain

$$[(1-\epsilon\bar{t})(1-\epsilon\bar{t}-\delta)\partial_{\bar{t}}-\delta(1-\epsilon\bar{x})\partial_{\bar{x}}+2\epsilon(1-\epsilon\bar{t}+\delta)] \times[(1-\epsilon\bar{t})(1-\epsilon\bar{t}-\delta)\partial_{\bar{t}}-\delta(1-\epsilon\bar{x})\partial_{\bar{x}}+\delta\epsilon]\tilde{\bar{n}}_e = -(1-\epsilon\bar{t}-\delta)^3(1-\epsilon\bar{t})(\tilde{\bar{n}}_b+\tilde{\bar{n}}_e)+2\epsilon^2\delta(1-\epsilon\bar{t}-\delta). \quad (14)$$

It will be shown later that the solutions to Eqs. (13) and (14) have the form $\tilde{\bar{n}}_j=a_j\exp[-i(\bar{t}-\bar{x})]$, $j=b,e$, where the slowly varying amplitudes a_j satisfy $|\partial_{\bar{t}}a_j|\gg\delta|a_j|$. In this case we can neglect all terms that contain δ in Eq. (14). We also assume that the perturbation amplitude is larger than the unneutralized charge density ($\tilde{\bar{n}}_e\gg\epsilon^2\delta$) represented by the last term in Eq. (14) [see also Eq. (8)], and therefore the last term in Eq. (14) can be neglected. Hence, Eqs. (13) and (14) can be simplified to give

$$[(1-\epsilon\bar{t})\partial_{\bar{t}}+(1-\epsilon\bar{x})\partial_{\bar{x}}-2\epsilon] \times[(1-\epsilon\bar{t})\partial_{\bar{t}}+(1-\epsilon\bar{x})\partial_{\bar{x}}-\epsilon]\tilde{\bar{n}}_b = -\alpha^2\epsilon^2(1-\epsilon\bar{t})(\tilde{\bar{n}}_e+\tilde{\bar{n}}_b), \quad (15)$$

$$\partial_{\bar{t}}^2\tilde{\bar{n}}_e+\tilde{\bar{n}}_e=-\tilde{\bar{n}}_b. \quad (16)$$

Next, we change variables from $\bar{x}$, $\bar{t}$ to

$$X=\epsilon\bar{x} \quad \text{and} \quad \tau=\bar{t}-\bar{x} \quad (17)$$

in Eqs. (15) and (16). With this change of variables, Eqs. (15) and (16) become

$$[(1-X)\partial_X-\tau\partial_\tau-2][(1-X)\partial_X-\tau\partial_\tau-1]\tilde{\bar{n}}_b = -\alpha^2(1-X-\epsilon\tau)(\tilde{\bar{n}}_e+\tilde{\bar{n}}_b), \quad (18)$$

$$(\partial_\tau^2+1)\tilde{\bar{n}}_e=-\tilde{\bar{n}}_b. \quad (19)$$

Substituting $\tilde{\bar{n}}_j=a_j\exp[-i\tau]$, $j=e,b$, into Eqs. (18) and (19), for $\tau\gg1$ we obtain the amplitude equation for a_e

$$[(1-X)\partial_X+\tau(i-\partial_\tau)]^2\partial_\tau(\partial_\tau-2i)a_e = -\alpha^2(1-X-\epsilon\tau)(\partial_\tau-i)^2a_e. \quad (20)$$

A similar equation can be obtained by substituting $kV_b=(\omega_{pe}/V_b^0-i\partial_x)\bar{V}_b(x,t)$ and $\omega=\omega_{pe}+i\partial_t$ into the two-stream dispersion relation for a beam-plasma system

$$\frac{\omega_{pe}^2}{\omega^2}+\frac{\omega_{pb}^2}{(\omega-kV_b)^2}=1. \quad (21)$$

The resulting equation is

$$\left[\frac{\partial}{\partial t}+V_b(x,t)\frac{\partial}{\partial x}+i\frac{\omega_{pe}}{V_b^0}[V_b(x,t)-V_b^0]\right]^2 \times\left(\frac{\partial}{\partial t}-2i\omega_{pe}\right)\frac{\partial a_e}{\partial t} = -\omega_{pb}^2(x,t)\left(\frac{\partial}{\partial t}-i\omega_{pe}\right)^2a_e(x,t). \quad (22)$$

Substituting Eqs. (5) and (6) into Eq. (22), we obtain Eq. (20). In the limit where $|\partial_X|\ll\tau$ and $|\partial_\tau|\ll1$, Eq. (20) can be integrated to give

$$a_e=c(X)\exp\left(i\alpha^2\frac{1-X+\epsilon\tau\log(\epsilon\tau)}{2\tau}\right). \quad (23)$$

It will be shown later that $\partial_X\sim\alpha$, and therefore both conditions $|\partial_X|\ll\tau$ and $|\partial_\tau|\ll1$ are equivalent to $\tau\gg\alpha$. To determine $c(X)$ in Eq. (23), we need to find a solution in the region $\tau\sim\alpha$ and then take the limit $\tau\gg\alpha$. In the region $\tau\sim\alpha$, we can neglect $\epsilon\tau\sim\delta^{1/2}\ll(1-X)$ in Eq. (18), which gives

$$[(1-X)\partial_X-\tau\partial_\tau-2][(1-X)\partial_X-\tau\partial_\tau-1]\tilde{\bar{n}}_b = -\alpha^2(1-X)(\tilde{\bar{n}}_e+\tilde{\bar{n}}_b), \quad (24)$$

$$(\partial_\tau^2+1)\tilde{\bar{n}}_e=-\tilde{\bar{n}}_b. \quad (25)$$

IV. ASYMPTOTIC SOLUTION

We now introduce the variable $Y=\log[1/(1-X)]$, and carry out the integral transform of Eqs. (24) and (25) according to $\tilde{\bar{n}}_e=\int_C ds\hat{n}_e(s,Y)\exp(-is\tau)$. This gives

$$[\partial_Y+s\partial_s-1][\partial_Y+s\partial_s](1-s^2)\hat{n}_e=\alpha^2\exp(-Y)s^2\hat{n}_e. \quad (26)$$

Here, use has been made of the fact that the integral transform of the operator $-\tau\partial_\tau\rightarrow\partial_s s=1+s\partial_s$. To solve Eq. (26), we introduce new variables $p=Y-\log(s)=\log[1/s(1-X)]$. In the new variables, Eq. (26) can be rewritten as

$$\partial_s^2\hat{n}_b=\alpha^2\frac{\exp(-p)}{s(1-s^2)}\hat{n}_b, \quad (27)$$

where use has been made of $\tilde{\bar{n}}_b=-(\partial_\tau^2+1)\tilde{\bar{n}}_e$, and therefore $\hat{n}_b=-(1-s^2)\hat{n}_e$. In obtaining Eqs. (26) and (27), it is assumed that the contour C is chosen so that the integrals exist and all integrand functions and their derivatives are zero on both ends of the contour C.

The WKB solution of Eq. (27) valid for $\alpha\gg1$ is given by

$$\hat{n}_b=\bar{b}_\pm(p)\exp\left[\pm2\alpha\exp(-p/2)\int_{\exp(-p/2)}^{\sqrt{s}}\frac{dz}{(1-z^4)^{1/2}}\right], \quad (28)$$

where $\bar{b}_\pm(p)$ are two arbitrary functions. Using Eq. (28), we can express the solution for $\tilde{\bar{n}}_b$ as

$$\tilde{\tilde{n}}_b = \sum_{\pm} \int_{C_\pm} ds f_\pm[s(1-X)] \times \exp\left[-i\tau s \pm 2\alpha s\sqrt{1-X} \int_{\sqrt{1-X}}^{1} \frac{dz}{(1-s^2z^4)^{1/2}} \right], \quad (29)$$

where the functions $f_\pm$ and integration contours $C_\pm$ are determined from the boundary conditions at $X=0$. Taking the limit $X\to 0$ in Eq. (29), we obtain

$$\tilde{\tilde{n}}_b(\tau,0) = \sum_{\pm} \int_{C_\pm} ds f_\pm(s)\exp(-i\tau s), \quad (30)$$

$$\partial_X \tilde{\tilde{n}}_b(\tau,0) = \sum_{\pm} \int_{C_\pm} ds \left[-sf'_\pm(s) \pm \alpha \frac{s}{\sqrt{1-s^2}} f_\pm(s) \right] \times \exp(-i\tau s). \quad (31)$$

The boundary condition consistent with $\tilde{\tilde{v}}_b(\tau, X=0)=0$ that follow from Eq. (10) are

$$\tilde{\tilde{n}}_b(\tau,0) = f(\tau)H(\tau), \quad (32)$$

$$\partial_X \tilde{\tilde{n}}_b(\tau,0) = (1+\tau\partial_\tau)\tilde{\tilde{n}}_b(\tau,0), \quad (33)$$

where $H(\tau)$ is the Heaviside step function defined by

$$H(\tau) = \begin{cases} 1 & \text{for } \tau \geqslant 1, \\ 0 & \text{for } \tau < 0. \end{cases} \quad (34)$$

Consistent with Eqs. (32) and (33) are the initial conditions and boundary conditions for the perturbed electron density, $\tilde{\tilde{n}}_e(\tau=0)=\partial_\tau \tilde{\tilde{n}}_e(\tau=0)=0$ and $(\partial_\tau^2+1)\tilde{\tilde{n}}_e(\tau, X=0)=-1$. The solution for $\tilde{\tilde{n}}_b$ that satisfies the boundary conditions in Eqs. (32) and (33) is given by

$$\tilde{\tilde{n}}_b = \int_{-\infty+i\Delta}^{+\infty+i\Delta} \frac{ds}{4\pi} \hat{f}[s(1-X)]\exp(-i\tau s) \times \sum_{\pm} \exp\left[\pm 2\alpha s\sqrt{1-X} \int_{\sqrt{1-X}}^{1} \frac{dz}{(1-s^2z^4)^{1/2}} \right], \quad (35)$$

where $\hat{f}(s)=\int_0^\infty d\tau \exp(is\tau)f(\tau)$, and Δ is such that the integration contour in Eq. (35) is above all singularities of the function $\hat{f}(s)$.

Since $\alpha \gg 1$ is assumed, the integral in Eq. (35) can be evaluated using the method of steepest descend. First, we shift the integration contour into the lower half-plane. The resulting contour C' is shown in Fig. 2. The contour C' goes around the cuts and poles of the integrand in Eq. (35). The main contribution to the integral is from the points where the function

$$H_\pm(s) = -is \pm 2\beta s\sqrt{1-X} \int_{\sqrt{1-X}}^{1} \frac{dz}{(1-s^2z^4)^{1/2}} \quad (36)$$

reaches an extremum. Here, we also take the limit $\beta=\alpha/\tau \ll 1$, which allows determination of the extremum points analytically. The function $H_\pm(s)$ has root branch points at $s_b^{\mathrm{I}}=\pm 1$ and $s_b^{\mathrm{II}}=\pm 1/\sqrt{1-X}$, and is analytic everywhere in the complex s plane with cuts made as shown in Fig. 2. The

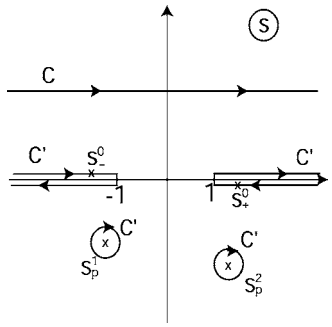

FIG. 2. Integration contour and location of extremum points for the functions $H_\pm(s)$ in Eq. (36).

imaginary part of the functions $H_\pm$ experience discontinuous jumps across the cuts. Equating the derivative to zero, $H'_\pm(s_0)=0$, we find that the extremum points are located near the branch points. One can show that only the extremum points near $s_b=\pm 1$ give exponentially growing contributions to the integral in Eq. (36). Expanding the functions $H_\pm(s)$ near $s\approx\pm 1$ and keeping leading-order terms in the small parameter β, we obtain

$$H_+(s \simeq +1) \simeq -is + \beta\sqrt{2(1-X)}F[\arccos(\sqrt{1-X})|1/2] - \beta\sqrt{2(1-X)}\sqrt{1-s}, \quad (37)$$

$$H_-(s \simeq -1) \simeq -is + \beta\sqrt{2(1-X)}F[\arccos(\sqrt{1-X})|1/2] - \beta\sqrt{2(1-X)}\sqrt{1+s},$$

where $F(x|\alpha)=\int_0^x d\theta/\sqrt{1-\alpha\sin^2\theta}$ is a elliptic integral of the first kind.

From $H'_\pm(s_\pm^0)=0$ we find that $s_+^0=1+\beta^2(1-X)/2$, which is located below the right cut, and $s_-^0=-1-\beta^2(1-X)/2$, which is located above the left cut, as shown in Fig. 2. The corresponding extremum values of the function $H_\pm(s_\pm^0)$ valid up to the second order in β are given by

$$H_\pm(s_\pm^0) = \mp i\left(1-\frac{\beta^2(1-X)}{2}\right) + \beta\sqrt{2(1-X)}F[\arccos(\sqrt{1-X})|1/2]. \quad (38)$$

With the same accuracy, it can be shown that $1/\sqrt{-H''_+(s_+^0)}=-\beta\sqrt{1-X}\exp(-i\pi/4)$ and $1/\sqrt{-H''_-(s_-^0)}=\beta\sqrt{1-X}\exp(i\pi/4)$. The extra minus sign multiplies the contribution from s_+^0 because the integration contour direction is reversed at this point. For the simple boundary condition in Eq. (32), $f(\tau)=1$, it follows that $\hat{f}(s)=i/s$ and we can express the asymptotic growing solution as

$$\tilde{\tilde{n}}_b(\tau,X) \simeq \frac{\alpha}{\sqrt{2\pi\tau^3(1-X)}} \sin[\tau-\alpha^2(1-X)/2\tau+\pi/4] \times \exp\{\alpha\sqrt{2(1-X)}F[\arccos(\sqrt{1-X})|1/2]\}. \quad (39)$$

The easiest way to determine $\tilde{\tilde{n}}_e(\tau,X)$ is to solve the equation

$$(\partial_\tau^2+1)\tilde{\tilde{n}}_e(\tau,X)=-\tilde{\tilde{n}}_b(\tau,X) \tag{40}$$

with initial conditions $\tilde{\tilde{n}}_e(0,X)=0$ and $\partial_\tau\tilde{\tilde{n}}_e(0,X)=0$, and with $\tilde{\tilde{n}}_b(\tau,X)$ given by Eq. (39). In the limit $\alpha\gg1$, the solution to Eq. (40) is given by

$$\tilde{\tilde{n}}_e(\tau,X)\simeq\frac{1}{2(1-X)}\,\mathrm{Re}\times\left\{\exp(i\tau)\left(1-\mathrm{erf}\left[\sqrt{\frac{i\alpha^2(1-X)}{2\tau}}\right]\right)\right\}\times\exp\{\alpha\sqrt{2(1-X)}F[\arccos(\sqrt{1-X})|1/2]\}, \tag{41}$$

where erf$[x]$ is the error function defined by $\mathrm{erf}[x]=(2/\sqrt{\pi})\int_0^x dx\exp(-x^2)$. The solutions in Eqs. (39) and (41) are valid far enough away from the beam head that $\tau\gg\alpha\sqrt{1-X}$. At the end of the compression, $t=T_f$ and $\tau=\alpha^2(1-X)$. At this time, the density perturbation can be expressed as

$$\tilde{\tilde{n}}_b(t=T_f,X)\simeq q_b\frac{\exp G(X)}{\alpha^2(1-X)^2}\sin[\alpha^2(1-X)+\pi/4-\phi_b], \tag{42}$$

$$\tilde{\tilde{n}}_e(t=T_f,X)\simeq q_e\frac{\exp G(X)}{(1-X)}\sin[\alpha^2\ (1-X))+\pi/4-\phi_e], \tag{43}$$

where the gain function $G(x)$ is defined by

$$G(X)=\alpha\sqrt{2(1-X)}F[\arccos(\sqrt{1-X})|1/2]. \tag{44}$$

In Eqs. (42) and (43) $q_b=1/\sqrt{2\pi}\approx0.40$, $\phi_b=1/2$, and $q_e\exp[-i(\phi_e+\pi/4)]=(1-\mathrm{erf}[\sqrt{i/2}])/2$. Numerically, we find $q_e\simeq0.29$ and $\phi_e\simeq0.12$.

V. PHYSICAL DISCUSSION

As evident from Eqs. (42) and (43), the saturated amplitude of the density perturbations is determined mostly by the gain function in Eq. (44). It is interesting to examine the development of the instability and its saturation from the point of view of wave dynamics where the plasma waves are represented as quasiparticles characterized by their position $x(t)$, wave number $k(t)$, and energy (or frequency) $\omega(t)$. The quasiparticle dynamics are described by the equations

$$\frac{dx}{dt}=\frac{\partial\omega}{\partial k}=-\frac{\partial D/\partial k}{\partial D/\partial w}, \tag{45}$$

$$\frac{dk}{dt}=-\frac{\partial\omega}{\partial x}=\frac{\partial D/\partial x}{\partial D/\partial w}, \tag{46}$$

$$\frac{d\omega}{dt}=\frac{\partial\omega}{\partial t}=-\frac{\partial D/\partial t}{\partial D/\partial w}, \tag{47}$$

where, for a beam propagating through background plasma, the dispersion function D is defined by

$$D=1-\frac{\omega_{pe}^2}{\omega^2}-\frac{\omega_{pb}^2(t)}{(\omega-kV_b(x,t))^2}, \tag{48}$$

and the quasiparticle dynamics is on the surface $D=0$. Substituting Eq. (48) into Eqs. (45)–(47), we obtain the closed system of equations for $x(t)$ and $p(t)=k(t)V_b(x,t)/\omega(t)$

$$\frac{dx}{dt}=\frac{V_b(x,t)}{1+(1-p)^3/\delta(t)}, \tag{49}$$

$$\frac{dp}{dt}=\left[p-\frac{p^2}{1+(1-p)^3/\delta(t)}\right]\frac{1}{V_b(x,t)}\frac{\partial V_b(x,t)}{\partial t}-\left[\frac{p(1-p)/2}{1+(1-p)^3/\delta(t)}\right]\frac{1}{\delta(t)}\frac{\partial\delta(t)}{\partial t}, \tag{50}$$

where $\delta(t)=\omega_{pb}^2(t)/\omega_{pe}^2$, and

$$\frac{\omega}{\omega_{pe}}=\left[1+\frac{1}{(1-p)^2/\delta(t)}\right]^{1/2}. \tag{51}$$

It follows from Eq. (51) that for $\delta\ll1$ the maximum growth rate occurs for $p\sim1$, which corresponds to perfect resonance. Equation (50) describes the detuning from resonance for particular quasiparticle under consideration. For a uniform noncompressing beam with $V_b=$const., Eqs. (49) and (50) are easily solved to give

$$p=p_0, \tag{52}$$

$$x-\frac{V_bt}{1+(1-p)^3/\delta}=x_0, \tag{53}$$

with the general solution $p(x,t)$ given by

$$x-\frac{V_bt}{1+(1-p)^3/\delta}=f(p). \tag{54}$$

We are interested in obtaining self-similar solutions which correspond to asymptotic solutions independent of the initial conditions. Such a solution is given by

$$(1-p)^3=\delta\left[\frac{V_bt-x}{x}\right]. \tag{55}$$

For $\delta^{1/3}[x/(V_bt-x)]^{2/3}\ll1$, we obtain from Eq. (51)

$$\frac{\omega}{\omega_{pe}}=1+\frac{(i\sqrt{3}-1)}{2}\frac{\delta^{1/3}}{2}\left[\frac{x}{V_bt-x}\right]^{2/3}, \tag{56}$$

where only the unstable solution with positive imaginary part of the frequency is retained. From Eq. (56), we obtain the gain function

$$G(x,t)=\int_{x/V_b}^{t}\mathrm{Im}\ \omega(x,\bar{t})d\bar{t}=\frac{3\sqrt{3}}{4}\frac{\omega_{pe}}{V_b}\delta^{1/3}x^{2/3}(V_bt-x)^{1/3}. \tag{57}$$

The gain function in Eq. (57) coincides with the gain function obtained by direct solution of the linearized fluid equations.[6] If follows from Eq. (57) that the gain function never saturates. This is because the quasiparticle's detuning $p-1$ does not change with time [see Eq. (52)], and quasipar-

ticles which were in resonance will stay in resonance indefinitely.

For the case where the beam velocity $V_b(x,t)$ changes dynamically according to Eq. (6), it follows that Eqs. (49) and (50) become

$$\frac{dp}{dT} = p - \frac{p(1+p)/2}{1+(1-p)^3/\delta}, \tag{58}$$

$$\frac{dY}{dT} = \frac{1}{1+(1-p)^3/\delta}, \tag{59}$$

where $Y=\log[1/(1-x/X_f)]$ and $T=\log[1/(1-t/T_f)]$. Introducing q defined by $p=1+q\delta^{1/3}$ in Eq. (58), we obtain equations for q valid to leading order in the small parameter δ, i.e.,

$$\delta^{1/3}\left(\frac{dq}{dT}+\frac{5}{6}q\right) = -q^3, \tag{60}$$

$$\frac{d\xi}{dT} = -q^3, \tag{61}$$

$$\frac{\omega}{\omega_{pe}} = \hat{\omega} = \left[1+\frac{\delta^{1/3}}{q^2}\right]^{1/2}, \tag{62}$$

where $\xi=T-Y$. As shown below, the instability in this case saturates when $q\sim\delta^{1/6}\ll 1$, which justifies retaining only leading-order terms in Eqs. (60) and (61). The solution to Eqs. (60) and (61) is given by

$$\exp(-2T)\left[\frac{\delta^{1/3}(T)}{q^2}+1\right] = I. \tag{63}$$

$$\xi = \xi_0 - \delta(T)^{1/2}\int_0^T d\bar{T}\frac{\exp[(\bar{T}-T)/2]}{[\exp\ (2\bar{T})I-1)]^{3/2}}, \tag{64}$$

where I and ξ_0 are invariants of the motion. Making use of Eqs. (62)–(64), we obtain the asymptotic solution for $\hat{\omega}(\xi,T)=\omega/\omega_{pe}$, which is independent on initial conditions, i.e.,

$$\xi = -2\delta(T)^{1/2}\int_{\exp(-T/2)}^1 \frac{d\eta}{[\ \eta^4\hat{\omega}^2-1)]^{3/2}}. \tag{65}$$

The gain function $G(x,\ t)$ is given by

$$G(x,t) = \int_{x/V_b}^t \mathrm{Im}\ \omega(x,\bar{t})d\bar{t}$$

$$= \omega_{pe}T_f\exp(-Y)\ \mathrm{Im}\int_0^\xi d\bar{\xi}\exp(-\bar{\xi})\hat{\omega}(\bar{\xi},Y). \tag{66}$$

It can be shown from Eq. (65) that $\mathrm{Im}\ \hat{\omega}\sim(\delta)^{3/2}/\xi^3$ for $\xi/\delta^{1/2}\gg 1$ so that we can neglect the exponential contribution in Eq. (66) to the integral, and also extend the upper integration limit to infinity for $\xi\gg\delta^{1/2}$. In addition, we can also replace $T\to Y$ on the right-hand side of Eq. (65). Integrating Eq. (66) by parts and taking into account that $\mathrm{Im}[\hat{\omega}(\xi)]\xi\sim 1/\xi^2\to 0$ for $\xi\to\infty$, and $\mathrm{Im}[\hat{\omega}(\xi)]\xi\sim\xi^{2/3}\to 0$ for $\xi\to 0$, we obtain

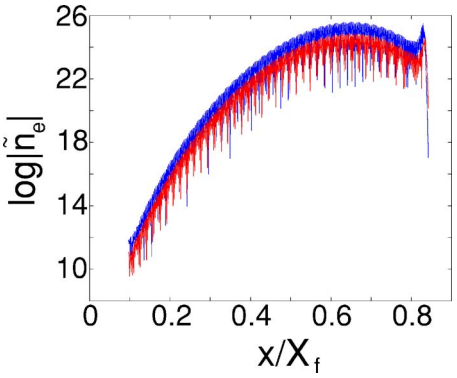

FIG. 3. (Color online) Logarithm of the electron density perturbation $\log|\tilde{n}_e|$ at time $t=0.85T_f$ plotted as a function of distance $X=x/X_f$. The lower (red) curve in is the numerical solution of the linearized fluid equations with no approximations and the upper (blue) curve is the numerical solution of the same equations with the approximation $(1-X-\epsilon\tau)\to(1-X)$ on the right-hand side of Eq. (18).

$$G = \omega_{pe}T_f\exp(-Y)\mathrm{Im}\int_0^\infty d\xi\hat{\omega}(\xi,Y)$$

$$= -\omega_{pe}T_f\exp(-Y)\mathrm{Im}\int_{\hat{\omega}(0,Y)}^{\hat{\omega}(\infty,Y)} d\hat{\omega}\xi(\hat{\omega},Y)$$

$$= -2\alpha\sqrt{1-X}\ \mathrm{Im}\int_{\sqrt{1-X}}^1 \frac{d\eta}{\sqrt{\eta^4-1/\hat{\omega}^2}}\Bigg|_{\hat{\omega}(0,Y)}^{\hat{\omega}(\infty,Y)}, \tag{67}$$

where $\alpha=\delta_0^{1/2}\omega_{pe}T_f=\omega_{pb}T_f$. Equation (65) has several solutions. The solution with positive imaginary part to the frequency, which corresponds to instability, corresponds to $\hat{\omega}^2(\infty,Y)=1$ and $\hat{\omega}^2(0,Y)=\infty$. Therefore, using Eq. (67), we obtain

$$G(X) = 2\alpha\sqrt{1-X}\int_{\sqrt{1-X}}^1 \frac{d\eta}{\sqrt{1-\eta^4}}$$

$$= \alpha\sqrt{2(1-X)}F[\arccos(\sqrt{1-X})|1/2], \tag{68}$$

where $X=x/X_f$. The gain function in Eq. (68) is identical to Eq. (44). The region where it is valid, $\xi\gg\delta^{1/2}$ or $\tau=\omega_p(t-x/V_b)\gg\alpha\sqrt{1-x/X_f}$, also coincides with the region where Eq. (44) is valid. The fact that we have obtained identical expressions for the gain function demonstrates the consistency of the approximations used in the derivations. The method of quasiparticles also clarifies the dynamics of the instability in a physically intuitive way.

VI. NUMERICAL SOLUTION

As anticipated in Eq. (23), the amplitude $c(X)=|a_e|\sim\exp(G)$ is primarily a function of X and satisfies $\partial_X\sim\alpha$. The gain function can be expressed as

$$G(X) = \alpha\sqrt{2(1-X)}F[\arccos(\sqrt{1-X})|1/2]. \tag{69}$$

To check the approximations, we have solved the linearized system of equations in Eqs. (13) and (14) numerically using the FEMLAB package.[15] For the numerical analysis the parameters are taken to be $\epsilon=1/(\omega_{pe}T_f)=10^{-3}$ and $\delta=n_b^0/n_0=10^{-3}$. These parameters correspond to $\alpha^2=\delta/\epsilon^2=(\omega_{pb}T_f)^2=1000$.

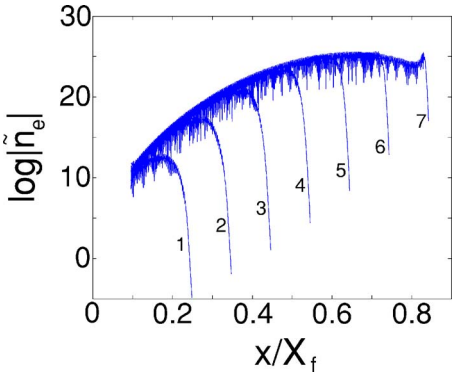

FIG. 4. Logarithm of the electron density perturbation $\log|\tilde{\bar{n}}_e|$ plotted as a function of distance x/X_f at different times t/T_f=0.25 (1), 0.35 (2), 0.45 (3), 0.55 (4), 0.65 (5), 0.75 (6), and 0.85 (7).

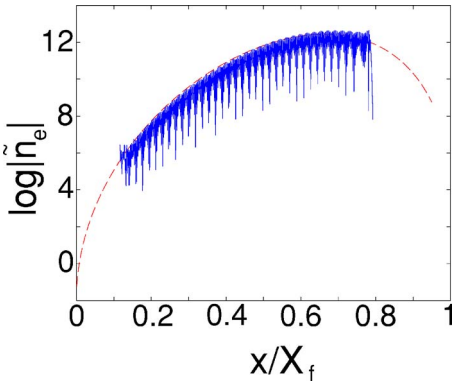

FIG. 6. (Color online) Logarithm of the electron density perturbation $\log|\tilde{\bar{n}}_e|$ plotted as a function of distance x/X_f at $t=0.80T_f$ obtained numerically (solid curve) and compared with the analytical result in Eq. (69) (dashed curve) for $\alpha^2=250$.

To compare with the theoretical results in Secs. IV and V, $f(\tau)=1$ is chosen for the boundary conditions in Eq. (32). The numerical results are shown in Figs. 3–7. Figure 3 shows the logarithm of the electron density perturbation, $\log|\tilde{\bar{n}}_e|$, at time $t=0.85T_f$ plotted as a function of the distance $X=x/X_f$. The lower (red) curve in Fig. 3 is the numerical solution of the linearized fluid equations with no approximations. The upper (blue) curve in Fig. 3 is the numerical solution of the same equations with the approximation $(1-X-\epsilon\tau)\rightarrow(1-X)$ on the right-hand side of Eq. (18). As evident from Fig. 3, this approximation does not change the space-time dependence of the solution, but only changes the overall amplitude slightly. Figure 4 illustrates the time dependence of the electron density perturbation $\log|\tilde{\bar{n}}_e(X,\tau)|$. The logarithm of the electron density perturbation $\log|\tilde{\bar{n}}_e|$ is plotted as a function of distance x/X_f at different times (1) t/T_f=0.25, (2) 0.35, (3) 0.45, (4) 0.55, (5) 0.65, (6) 0.75, and (7) 0.85. It is evident from the Fig. 4 that the amplitude, $|\tilde{\bar{n}}_e(X,\tau)|$, is indeed only a function of X away from the beam head where $\tau>\alpha\sqrt{1-X}$. Figure 5 shows the logarithm of the electron density perturbation, $\log|\tilde{\bar{n}}_e|$, plotted as a function of distance $X=x/X_f$ at $t=0.85T_f$ obtained numerically and compared with the analytical solution in Eq. (69). As evident from Fig. 5, the agreement is very good. The gain function in Eq. (69) scales linearly with parameter $\alpha=\omega_{pb}T_f$. This scaling is confirmed in Fig. 6 where the logarithm of the electron density perturbation, $\log|\tilde{\bar{n}}_e|$, is plotted as a function of distance $X=x/X_f$ at $t=0.80T_f$, together with the analytical solution for the case where the beam density is reduced by a factor of 4 ($\alpha^2=250$) compared to the case shown in Fig. 5. Figure 7 shows a comparison of the gain function in Eq. (69) with the gain function for a beam with zero velocity tilt [Eq. (70)], i.e.,

$$G_{\text{no tilt}}(X,t=T_f)=\alpha\frac{3\sqrt{3}}{4}\frac{X^{2/3}(1-X)^{1/3}}{\delta^{1/6}}. \tag{70}$$

As evident from Fig. 7, for $\delta^{1/6}\ll 1$ the velocity tilt significantly reduces the growth rate compared to the case of a beam with zero initial velocity tilt.

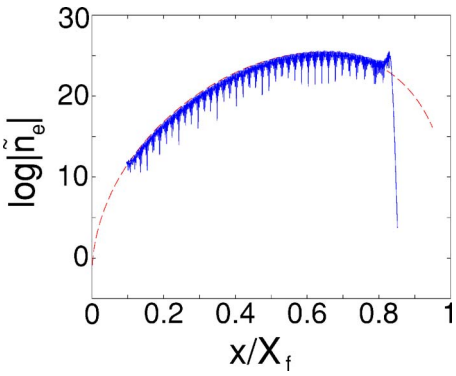

FIG. 5. (Color online) Logarithm of the electron density perturbation $\log|\tilde{\bar{n}}_e|$ plotted as a function of distance x/X_f at $t=0.85T_f$ obtained numerically (solid curve) and compared with the analytical result in Eq. (69) (dashed curve).

VII. CONCLUSIONS

The electrostatic two-stream instability for a cold, longitudinally compressing electron beam propagating through a background plasma has been investigated both analytically and numerically. Small-signal coupled equations describing the evolution of the density perturbations were derived, and the asymptotic solutions were obtained. The results were confirmed by direct numerical solution of the linearized fluid

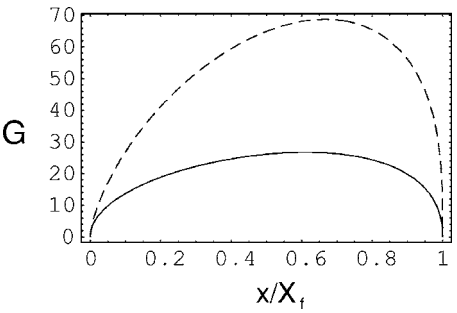

FIG. 7. Comparison of the instability gain as a function of x/X_f for a beam with (solid curve) and without (dashed curve) velocity tilt for $\delta=n_b^0/n_0=10^{-3}$ and $\alpha^2=(\omega_{pb}T_f)^2=1000$.

equations. It was shown that the longitudinal beam compression strongly modifies the space-time development of the instability. In particular, the dynamic compression leads to a significant reduction in the growth rate of the two-stream instability compared to the case without an initial velocity tilt by a factor $G_{\max}/G_{\max}^{\text{no tilt}} \sim (\omega_{pb}/\omega_{pe})^{1/3} \ll 1$. The number of e-foldings is proportional to the number of beam-plasma periods $1/\omega_{pb}$ during the compression time T_f. The two-stream instability is completely mitigated by the effects of dynamical beam compression when $\omega_{pb} T_f \lesssim 1$.

In the present, we considered the case of a semi-infinite beam (see Fig. 1). For a beam with finite initial length L_b^0, the trailing beam end will trace the trajectory $x_{\text{end}}(t) = V_b^0 t [1 + L_b^0/X_f] - L_b^0$. In this case, the present analysis is applicable everywhere between the leading and trailing edges of the beam, $\max\{0, x_{\text{end}}(t)\} \leqslant x \leqslant x_{\text{head}}(t) = V_b^0 t$, where the beam can drive the background plasma unstable. Behind the beam, for $0 \leqslant x < x_{\text{end}}(t)$ the plasma will be left with remnant collective oscillations with constant amplitude, which are excited by the propagating beam.

The full neutralization assumption is also violated at the beam head, where the time-changing magnetic field induces a longitudinal electric field which acts on the plasma electrons to cause a flow of return current opposite to the injected current. The distance from the beam head where the current and charge neutrality conditions are violated depends on the smoothness of the beam head density profile.[16] Generally, if the density profile of the beam increases from zero to its maximum value over a distance larger than V_{b0}/ω_{pe}, the beam charge is fully neutralized. In addition, the beam current will be neutralized if the beam diameter is much larger than the collisionless skin-depth c/ω_{pe}.

In this paper, we considered only low-density electron beam propagation in a background plasma. In this case, the unstable interaction is between the beam electrons and the plasma electrons. In the general case of a beam with arbitrary charge species and mass, the instability may also involve the background plasma ions, because of the nonzero relative velocity between the background ions and the neutralizing plasma electrons. This will occur if the beam ions are sufficiently heavy that the beam plasma frequency is smaller than the background ion plasma frequency, $\omega_{pb} \ll \omega_{pi}$. In this case, the two-stream instability between the background plasma electrons and the background plasma ions is expected to lead to a heating of the background electrons to thermal velocities comparable with the average flow velocity of the neutralizing background electrons $\sim (n_b/n_e) V_b$. During this initial stage, the beam ions are relatively unaffected. At later times, a two-stream instability between the beam ions and the (heated) background electrons may develop. This later stage of instability, which directly affects the beam particles, can also be described by the analysis presented in this paper.

ACKNOWLEDGMENT

This research was supported by the U. S. Department of Energy.

[1] E. A. Startsev and R. C. Davidson, New J. Phys. **6**, 141 (2004).
[2] P. K. Roy, S. S. Yu, E. Henestroza *et al.*, Phys. Rev. Lett. **95**, 234801 (2005).
[3] D. R. Welch, D. V. Rose, T. C. Genoni, S. S. Yu, and J. J. Barnard, Nucl. Instrum. Methods Phys. Res. A **544**, 236 (2005).
[4] P. K. Roy, S. S. Yu, S. Eylon *et al.*, Phys. Plasmas **11**, 2890 (2004).
[5] C. Thoma, D. R. Welch, S. S. Yu, E. Henestroza, P. K. Roy, S. Eylon, and E. P. Gilson, Phys. Plasmas **12**, 043102 (2005).
[6] R. Briggs, in *Advances in Plasma Physics*, edited by A. Symon and W. B. Thompson (Interscience, New York, 1971), Vol. 4, p. 43.
[7] R. C. Davidson, I. Kaganovich, H. Qin, E. A. Startsev, D. R. Welch, D. V. Rose, and H. S. Uhm, Phys. Rev. ST Accel. Beams **7**, 114801 (2004).
[8] H. Qin, E. A. Startsev, and R. C. Davidson, Phys. Rev. ST Accel. Beams **6**, 014401 (2003).
[9] H. Qin, Phys. Plasmas **10**, 2708 (2003).
[10] R. C. Davidson and H. Qin, *Physics of Intense Charged Particle Beams in High Energy Accelerators* (World Scientific, Singapore, 2001), and references therein.
[11] D. D. Ryutov, Sov. Phys. JETP **30**, 131 (1970).
[12] E. P. Lee, Simon Yu, H. L. Buchanan, F. W. Chambers, and M. N. Rosenbluth, Phys. Fluids **23**, 2095 (1980).
[13] T. C. Genoni, D. V. Rose, D. R. Welch, and E. R. Lee, Phys. Plasmas **11**, L73 (2004).
[14] P. Stroud, Laser Part. Beams **4**, 261 (1986).
[15] FEMLAB Reference Manual, Comsol AB, Stockholm, Sweden, version 2.2 ed. (2001).
[16] I. Kaganovich, E. A. Startsev, and R. C. Davidson, Phys. Plasmas **11**, 3546 (2004).